

## Article

# Microstructure and Magnetic Properties of Nanocrystalline Fe<sub>60-x</sub>Co<sub>25</sub>Ni<sub>15</sub>Si<sub>x</sub> Alloy Elaborated by High-Energy Mechanical Milling

Nawel Khitouni <sup>1,2</sup>, Béchir Hammami <sup>3</sup> , Núria Llorca-Isern <sup>4</sup> , Wael Ben Mbarek <sup>2</sup>, Joan-Josep Suñol <sup>2,\*</sup>  and Mohamed Khitouni <sup>3</sup>

<sup>1</sup> Laboratory of Inorganic Chemistry (LR17ES07), Faculty of Sciences of Sfax, University of Sfax, Sfax 3029, Tunisia

<sup>2</sup> Department of Physics, University of Girona, Campus Montilivi, 17071 Girona, Spain

<sup>3</sup> Department of Chemistry, Qassim University, Buraidah 51452, Saudi Arabia

<sup>4</sup> Department of CM-QE, Universitat de Barcelona, Martí Franquès 1, 08028 Barcelona, Spain

\* Correspondence: joanjosep.sunyol@udg.edu; Tel.: +34-972419757

**Abstract:** In the present work, the effect of Si addition on the magnetic properties of Fe<sub>60-x</sub>Co<sub>25</sub>Ni<sub>15</sub>Si<sub>x</sub> (x = 0, 5, 10, 20, and 30 at%) alloys prepared by mechanical alloying was analyzed by X-ray diffraction and magnetic vibrating sample magnetometry and SQUID. The crystallographic parameters of the bcc-solid solutions were calculated by Rietveld refinement of the X-ray diffraction patterns with Maud software. Scanning electron microscopy (SEM) was used to determine the morphology of the powdered alloys as a function of milling time. It was found that the Si addition has an important role in the increase of structural hardening and brittleness of the particles (favoring the more pronounced refinement of crystallites). The resulting nanostructure is highlighted in accordance with the concept of the structure of defects. Magnetic properties were related to the metalloid addition, formed phases, and chemical compositions. All processed samples showed a soft ferromagnetic behavior (H<sub>c</sub> ≤ 100 Oe). The inhomogeneous evolution of the magnetization saturation as a function of milling time is explained by the magnetostriction effective anisotropy and stress induced during mechanical alloying.

**Keywords:** mechanical alloying; Fe-Co-Ni-Si alloy; magnetic properties



**Citation:** Khitouni, N.; Hammami, B.; Llorca-Isern, N.; Mbarek, W.B.; Suñol, J.-J.; Khitouni, M. Microstructure and Magnetic Properties of Nanocrystalline Fe<sub>60-x</sub>Co<sub>25</sub>Ni<sub>15</sub>Si<sub>x</sub> Alloy Elaborated by High-Energy Mechanical Milling. *Materials* **2022**, *15*, 6483. <https://doi.org/10.3390/ma15186483>

Academic Editor: Francesco Iacoviello

Received: 18 July 2022

Accepted: 13 September 2022

Published: 19 September 2022

**Publisher's Note:** MDPI stays neutral with regard to jurisdictional claims in published maps and institutional affiliations.



**Copyright:** © 2022 by the authors. Licensee MDPI, Basel, Switzerland. This article is an open access article distributed under the terms and conditions of the Creative Commons Attribution (CC BY) license (<https://creativecommons.org/licenses/by/4.0/>).

## 1. Introduction

Fe–Co-based alloys are of great interest because they have good soft magnetic behavior such as high specific saturation magnetization, high permeability, and elevated Curie temperature that make them attractive for high-temperature applications and suitable for magnetic recording and magnetic fluids [1–4]. Fe–Ni alloys are promising candidates for wide applications in technology since they exhibit good soft properties but have low resistivity [5–7]. In recent years, there is a great demand for soft magnetic materials such as steels with high carbon or silicon which are brittle at room temperature. However, it has been found that adding Ni to Fe–Co materials improves permeability and resistivity at the same time [8]. As a result, the Fe–Ni–Co alloys are required for applications as soft magnetic materials because of their higher saturation magnetization (M<sub>s</sub>), lower coercivity (H<sub>c</sub>), and high resistivity. Moreover, the addition of a certain amount of B, C, P, and Si to α-Fe-based alloys has been shown to promote thermal and soft magnetic properties [9,10]. Mechanical alloying (MA) is an interesting technique used to prepare amorphous or nanostructured magnetic alloys and even to produce metastable phases of immiscible systems. Significant changes in the microstructure during the high-energy mechanical alloying can greatly affect the magnetic properties [11]. The thermal relaxation of the stress that occurred during the milling process can cause an increase of saturation magnetization (M<sub>s</sub>) and a

decrease of coercivity ( $H_c$ ). It has been reported that the magnetic properties of an alloy are related to the basic metal mixture, the alloying elements, and the crystal structures [12–17]. Indeed, saturation magnetization depends on the compositional and structural changes, and resulting phase constitution [18], while  $H_c$  is linked to the grain size, the defects density, impurities, and lattice strains [19]. Research works have investigated the important role of microstructure and phase transformation, that occurred during milling, on the changes in the magnetic properties of Fe-based alloys [18–24] and studied their restricted applications. The investigation of structural defects' role in nanostructure and magnetic behaviors seems useful for understanding their correlation with microstructure and phase transformations in Fe-based alloys. The crystalline defects introduced in terms of dislocations, grain boundaries, stacking defects, etc., during high-energy milling must be mentioned as the main causes for the enhancement of the magnetic properties of these compounds. For that, the comprehension of the relationship structure defects' magnetic behavior could be considered among the current topics of research. The main objective of this work can be briefly explained as follows: we presented a mechanosynthesis of ternary FeCoNi doped with Si for the comprehension of the Si addition's influence on the microstructure and magnetic behavior. The representation of the variation of the magnetic parameters according to those of the microstructure may facilitate the comprehension of the important role of structural defects in good magnetic properties. In this work, the compositions  $Fe_{60-x}Co_{25}Ni_{15}Si_x$  ( $x = 0, 5, 10, 20,$  and  $30$  at.%) were synthesized by high-energy mechanical alloying to find out the effect of both the Si addition and the structural defects in the magnetic behavior of the alloy.

## 2. Materials and Methods

The elemental powders of Fe (99.97% purity, mean particle size  $< 10 \mu m$ ), Co (99.9% purity, mean particle size  $< 2-5 \mu m$ ), Ni (99.7% purity, mean particle size  $< 10 \mu m$ ), and Si (99.5% purity, mean particle size  $< 10 \mu m$ ) were mechanically alloyed in an Ar atmosphere to synthesize the  $Fe_{60-x}Co_{25}Ni_{15}Si_x$  ( $x = 0, 5, 10, 20,$  and  $30$ ) (at.%) powders by using a planetary ball mill (Fritsch P7). The ball-to-powder weight ratio was chosen to be 2:1, and the milling intensity was set at 600 rpm. The milling was handled up to 100 h with a sequence consisting of 10 min of milling followed by 5 min of an idle period, to prevent the powder from sticking to the walls of the container and the balls and its agglomeration during milling. X-ray diffraction (XRD) patterns were collected using a D-500 Siemens equipment with  $CuK\alpha$  radiation ( $\lambda = 0.15406$  nm). The microstructural parameters such as crystallites size, lattice strains, and lattice parameter were obtained by Rietveld refinement using the Maud program [25]. In all refined XRD patterns, quality refinement parameter  $R_{exp}$  is lower than 10.5% and GOF parameter lower than 1.6. The morphology and the composition of MA powders were determined by scanning electron microscopy (SEM) in a DSM960A ZEISS microscope in secondary electron mode operating at a voltage of 15 kV. The SEM was equipped with a Vega-Tescan energy dispersive X-ray spectrometry (EDS) analyzer. The magnetic characterization was carried out by Superconducting Quantum Interference Device from Quantum Design SQUID MPMS-XL at 300 K.

## 3. Results and Discussion

### 3.1. SEM Analysis

Figure 1 gives typical examples of the SEM images of the alloyed  $Fe_{55}Co_{25}Ni_{15}Si_5$  and  $Fe_{30}Co_{25}Ni_{15}Si_{30}$  powder mixtures obtained after 4 and 100 h of milling. The particle size was reduced from around  $7 \mu m$  in both samples with increased milling time up to 100 h. Two deformation mechanisms are responsible for the final microstructure: plastic deformation (associated with cold welding in ductile powders and fracture in hard powders) [26,27]. Indeed, the Si particles are harder and more brittle than iron, cobalt, and nickel particles, so they are fractured and the small ones have consolidated to the lamellar particles, and then agglomerated particles with different sizes and shapes are formed [28]. Figure 1a,c shows the morphology of the 4 h powders; the particles appear

fine ( $\sim 7 \mu\text{m}$ ) and less agglomerated. This state can be related to the compressive forces introduced into the deformed particles after the successive ball–powder–ball collisions show that for all compositions and powders, larger particles with irregular shapes and sizes are formed due to cold welding. After an increase in milling up to 100 h, particles appear in spherical shapes and more uniform size distribution, as a result of intensive fracture after a preliminary cold-welding stage. This is due to the dissolution of Si in the metallic matrix indicating that the alloying process will take place (Figure 1b,d). Moreover, an increase in milling time leads to a work hardening (due to mechanically induced crystallographic defects) of the particles, and then fracturing occurs. In addition to the milling time, the competition between fracturing and welding processes under the effect of severe plastic deformation depends on the silicon content. In fact, at low content, metallic particles are soft and malleable and tend to weld together and form an agglomerate particle (larger particles), whereas for high Si content, the particles get work-hardened and tend to fracture, and the size of the particles diminishes (Figure 1b,d).

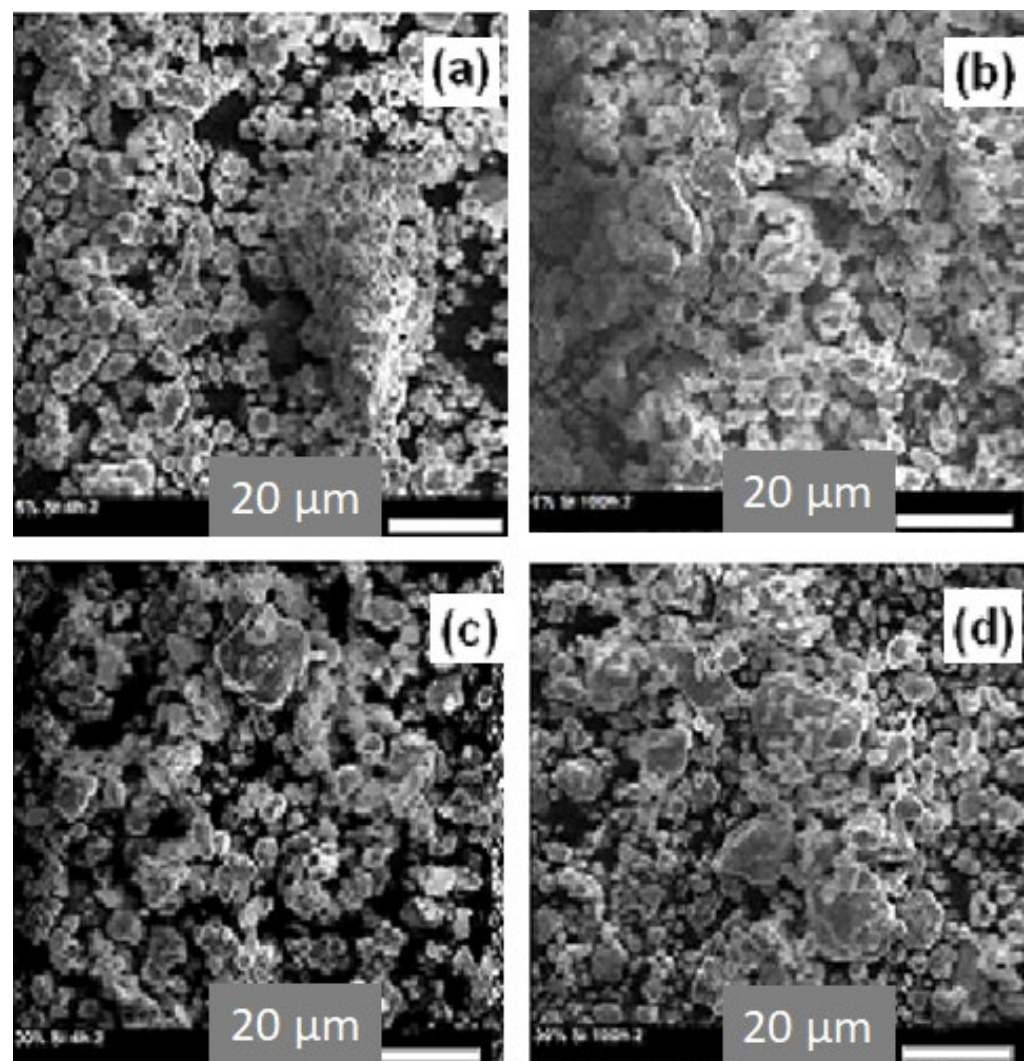


**Figure 1.** SEM micrographs for powders:  $\text{Fe}_{55}\text{Co}_{25}\text{Ni}_{15}\text{Si}_5$  obtained after 4 h (a) and after 100 h of milling (b) and  $\text{Fe}_{30}\text{Co}_{25}\text{Ni}_{15}\text{Si}_{30}$  milled for 4 h (c) and for 100 h (d), respectively.

Figure 2 shows the EDS analysis of the powder mixtures containing 5 and 30% Si milled for 100 h, respectively. Microanalysis confirms that the percentage ratio of the original elements is very close to the nominal values in both cases (56.35at%Fe-24.1at%Co-14.8at%Ni-4.75at%Si and 31.48at%Fe-25.1at%Co-14.3at%Ni-29.12at%Si). Nevertheless, EDS also reveals the existence of some traces of oxygen as well as the four mixture elements.

This may be the cause of contact of the milled powder with the oxygen in the air during its collection from jars.

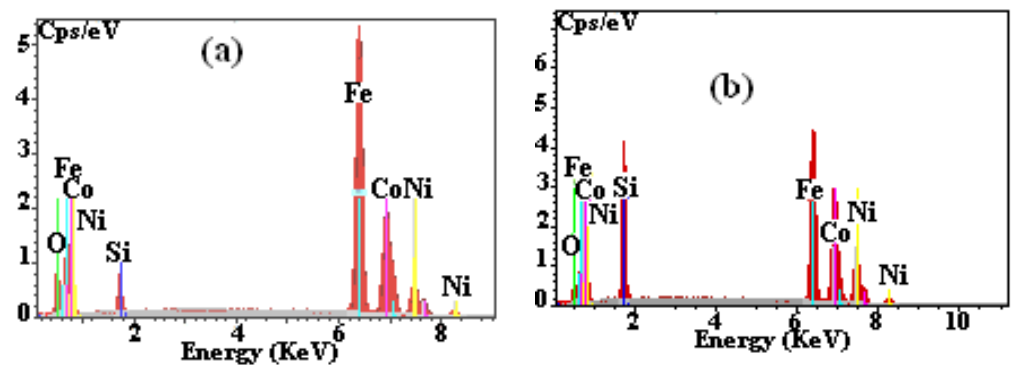


Figure 2. EDS spectra of milled (100 h) powdered alloys:  $\text{Fe}_{55}\text{Co}_{25}\text{Ni}_{15}\text{Si}_5$  (a) and  $\text{Fe}_{30}\text{Co}_{25}\text{Ni}_{15}\text{Si}_{30}$  (b).

### 3.2. XRD Analysis

The structure and phases evolution of  $\text{Fe}_{60-x}\text{Co}_{25}\text{Ni}_{15}\text{Si}_x$  powders ( $x = 0, 5, 10, 20$  and  $30$  at.%) were examined according to the milling time. The Rietveld analysis of the XRD patterns of alloys containing 5, 10, 20, and 30 at.% of Si, obtained after 2, 50, and 100 h of milling, are shown in Figure 3. The goodness of fit (GOF) refinement parameter was always  $<1.23$ .

The refinement of the XRD diffractograms of the powder with 5%Si, milled for 2 h, identifies the following phases: basic bcc-iron ( $\text{Im-3m}$ ;  $a = 2.8665(1) \text{ \AA}$ ; wt(%)~55), hcp-cobalt ( $\text{P63/mmc}$ ;  $a = 2.5057(1) \text{ \AA}$  and  $c = 4.0713(1) \text{ \AA}$ ; wt(%)~25), fcc-nickel ( $\text{Fm-3m}$ ;  $a = 3.5245(1) \text{ \AA}$ ; wt(%)~15), and cubic-silicon ( $\text{Fd-3m}$ ;  $a = 5.4355(2) \text{ \AA}$ ; wt(%)~5) (Figure 3a). Prolonging the milling time up to 50 h, we remark the appearance of the bcc-Fe(Co,Ni,Si) supersaturated solid solution with lattice parameters  $2.8661(1) \text{ \AA}$  and phase proportion around 51%. After 100 h milling, the final milling product is multiphase where the refined phases are the bcc-Fe(Co,Ni,Si) ( $\text{Im-3m}$ ;  $a = 2.8663(1) \text{ \AA}$ ; wt(%)~62) and some proportions of the hcp-cobalt ( $\text{P63/mmc}$ ;  $a = 2.5040(1) \text{ \AA}$  and  $c = 4.0684(1) \text{ \AA}$ ; wt(%)~7), fcc-nickel ( $\text{Fm-3m}$ ;  $a = 3.5239(1) \text{ \AA}$ ; wt(%)~7), and cubic-silicon ( $\text{Fd-3m}$ ;  $a = 5.4322(2) \text{ \AA}$ ; wt(%)~6) which still remain free. At the same time, we refined some traces of iron oxides in the forms  $\text{Fe}_2\text{O}_3$  ( $\text{R-3C}$ ;  $a = 5.0355(2)$  and  $c = 13.7471(1) \text{ \AA}$ ; wt(%)~8) and  $\text{Fe}_3\text{O}_4$  ( $\text{Fd-3m}$ ;  $a = 8.3967(2) \text{ \AA}$ ; wt(%)~10). In the case of the mixture of powders containing 10% Si, the Rietveld refinement confirms the formation of the solid solution bcc-FeCo ( $\text{Im-3m}$ ;  $a = 2.8687(1) \text{ \AA}$ ; wt(%)~20) after 2 h, while after 50 h, Co as a free element disappears completely by entering into the Fe lattice to form the bcc-Fe(Co,Ni,Si) ( $\text{Im-3m}$ ;  $a = 2.8623(1) \text{ \AA}$ ; wt(%)~88) supersaturated solid solution with a small proportion of the fcc-Ni(Si) ( $\text{Fm-3m}$ ;  $a = 3.5337(1) \text{ \AA}$ ; wt(%)~12) (Figure 3b). After 100 h of milling, we identify only the phase bcc-Fe(Co,Ni,Si) ( $\text{Im-3m}$ ;  $a = 2.8563(1) \text{ \AA}$ ; wt(%)~100).

For the compound with 20% Si (Figure 3c), the substitution of cobalt in the iron matrix to form the bcc-Fe(Co) phase is identified after a milling time of 50 h. A good Rietveld refinement shows the coexistence of the Fe(Co) phase ( $\text{Im-3m}$ ;  $a = 2.8675(1) \text{ \AA}$ ; wt(%)~65) with the free elements cobalt ( $\text{P63/mmc}$ ;  $a = 2.5057(1) \text{ \AA}$  and  $c = 4.0694(1) \text{ \AA}$ ; wt(%)~15), nickel ( $\text{Fm-3m}$ ;  $a = 3.5237(1) \text{ \AA}$ ; wt(%)~13), and silicon ( $\text{Fd-3m}$ ;  $a = 5.4293(2) \text{ \AA}$ ; wt(%)~7). The same phases are also refined after 100 h of milling. For a sample with 30% Si, the formation of the Fe(Co) solid solution ( $\text{Im-3m}$ ;  $a = 2.8692(1) \text{ \AA}$ ; wt(%)~55) was observed after 2 h milling (Figure 3d). After 50 h of milling, Rietveld refinement was successful by three phases: Fe(Co,Si) ( $\text{Im-3m}$ ;  $a = 2.8530(1) \text{ \AA}$ ; wt(%)~62.5) and Fe(Ni) ( $\text{Im-3m}$ ;  $a = 2.8670(1) \text{ \AA}$ ; wt(%)~31) solid solutions with silicon ( $\text{Fd-3m}$ ;  $a = 5.3670(1) \text{ \AA}$ ; wt(%)~6.5) (Figure 4c), while the hcp-Co has completely disappeared in the Fe lattice. At 100 h of milling, two metallurgical states were identified: an amorphous phase (proportion~65%) and a Fe(Co,Ni,Si) solid solution ( $\text{Im-3m}$ ;  $a = 2.8526(1) \text{ \AA}$ ; wt(%)~35).

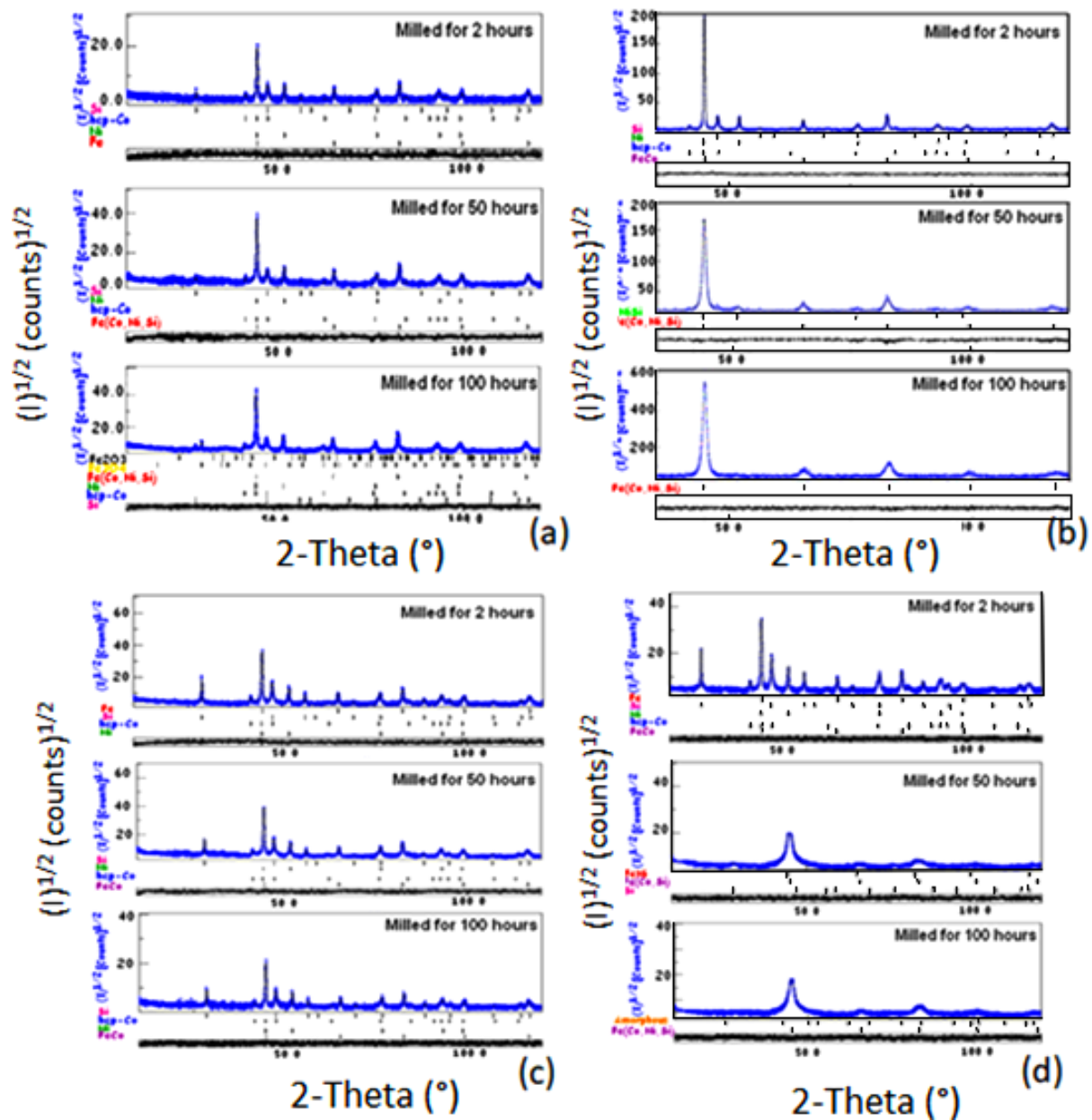


**Figure 3.** XRD diffractograms (experimental, refinement) of powdered mixtures containing 5 (a), 10 (b), 20 (c), and 30 (d) at.% Si. Alloys are milled for 2, 50, and 100 h.

Table 1 shows the microstructural parameters of the bcc-phase main phase as a function of milling time. The crystallite size of elemental Fe obtained before milling was about 150 nm. After the first 2 h of milling, the solid solution is formed and a rapid decrease of size (<80 nm) is observed. With continuing the milling up to 50 h, additional crystallite size refinement occurs slowly to a value of 33 nm in the samples with 5%Si and down to a value of 17 nm for the powder with 30%Si. After 100 h of milling, the refined average crystallite size was around 10 nm for the sample with 30%Si and 20 nm for the sample containing lower Si content.

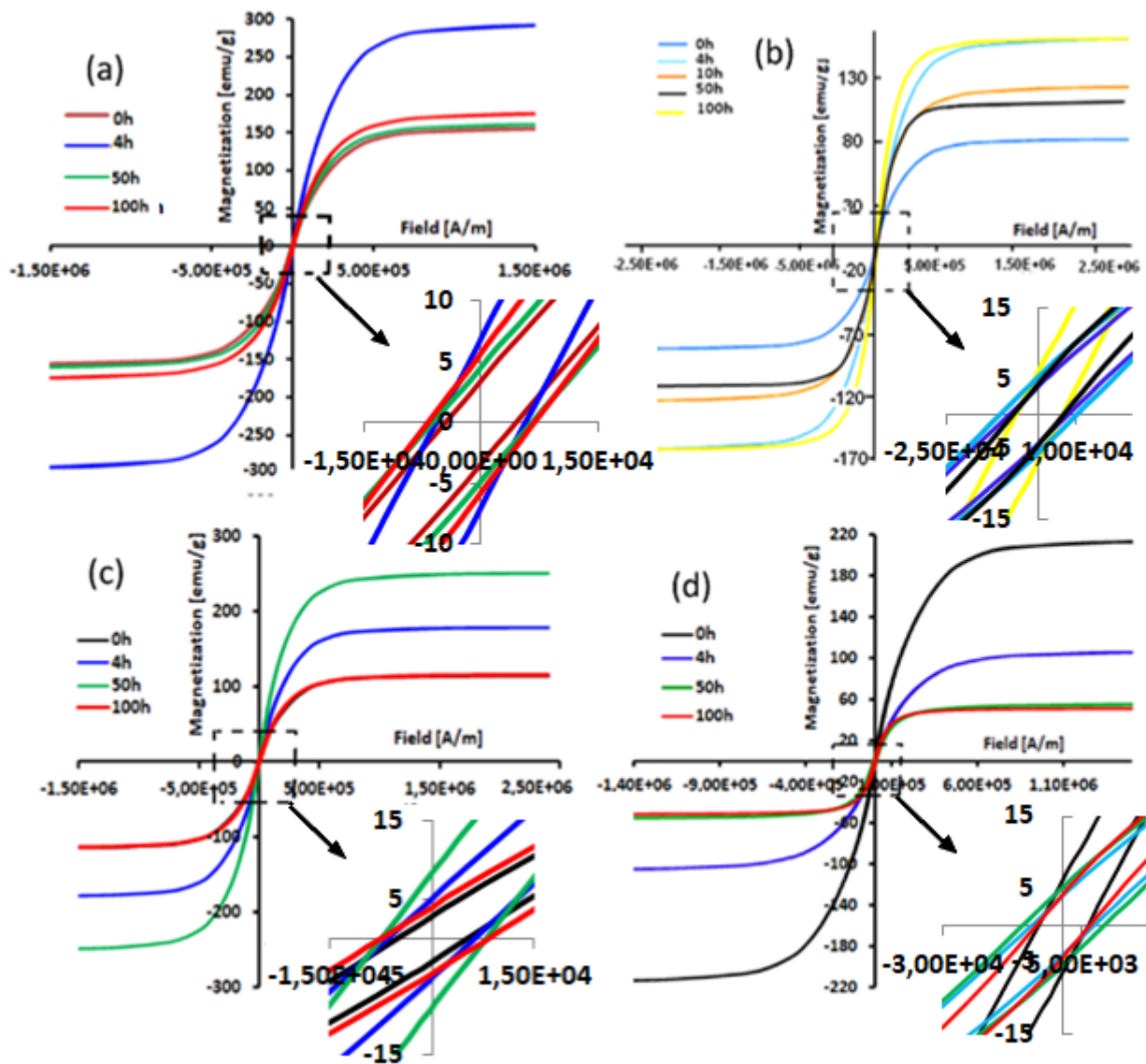


**Figure 4.** Typical hysteresis cycles (at 300 K) of the MA  $Fe_{60-x}Co_{25}Ni_{15}Si_x$  alloys:  $x = 5$  (a),  $x = 10$  (b),  $x = 20$  (c), and  $x = 30$  (d) at.% for selected milling times. (Units:  $1 \text{ emu/g} = 1 \text{ Am}^2\text{Kg}$ ). Notation: E+06 corresponds to  $\times 10^6$ , symbol—correspond to minus.

**Table 1.** Refined average crystallite sizes,  $\langle D \rangle$  ( $\pm 5 \text{ nm}$ ), lattice strains,  $\epsilon$  ( $\pm 0.02\%$ ), and dislocation density,  $\rho_{bcc}$  ( $\pm 0.05 \times 10^{15} \text{ m}^{-2}$ ), for  $Fe_{60-x}Co_{25}Ni_{15}Si_x$  powders ( $x = 0, 5, 10, 20,$  and  $30$  at.%).

t(h)	$Fe_{55}Co_{25}Ni_{15}Si_5$			$Fe_{50}Co_{25}Ni_{15}Si_{10}$			$Fe_{40}Co_{25}Ni_{15}Si_{20}$			$Fe_{30}Co_{25}Ni_{15}Si_{30}$		
	$\langle D \rangle$ (nm)	$\epsilon$ (%)	$\rho_{bcc}$ ( $m^{-2}$ ) $\times 10^{15}$	$\langle D \rangle$ (nm)	$\epsilon$ (%)	$\rho_{bcc}$ ( $m^{-2}$ ) $\times 10^{15}$	$\langle D \rangle$ (nm)	$\epsilon$ (%)	$\rho_{bcc}$ ( $m^{-2}$ ) $\times 10^{15}$	$\langle D \rangle$ nm	$\epsilon$ (%)	$\rho_{bcc}$ ( $m^{-2}$ ) $\times 10^{15}$
0	150	0.005	0.046	150	0.005	0.046	150	0.005	0.046	150	0.005	0.046
2	74	0.12	0.16	75	0.14	0.16	78	0.18	0.23	80	0.25	0.26
4	65	0.25	0.48	70	0.15	0.27	75	0.20	0.35	76	0.35	0.41
10	55	0.29	0.73	50	0.38	1.05	47	0.45	1.3	38	0.5	1.8
25	41	0.35	1.1	38	0.65	2.3	35	0.55	2.1	25	0.65	3.3
50	33	0.88	3.7	30	0.91	4.2	25	0.98	5.4	17	1.05	9.8
80	27	0.87	4.4	25	0.95	5.3	20	1.02	6.9	12	1.20	14.07
100	20	0.95	5.3	17	1.05	7.3	15	1.1	8.5	10	1.25	17.5

In all compositions, the decrease of crystallite size is greater in the first step of mechanical alloying, while further milling slightly diminishes the crystallite size. This behavior can be related to the work-hardening stage which increases defects density (grains boundaries, dislocations, etc.). At the extended stages of the milling process, a remarkable transition from work-hardening to layered nanostructures regions may occur. When severe deformation takes place, the dislocation density tends towards a small critical value which may cause subsequent recrystallization, and for that, the size of the crystallite varies slowly. In addition, one can observe that the crystallite size of a powder with 30% Si appears smaller and thinner than other samples. This behavior hints that the solid solutions become harder with the addition of Si, which creates further fragmentation of the particles and, consequently, the obtention of small crystals [29]. In parallel, the microstrains increase as a function of milling time. This increase may be linked to the formation and movement of the dislocations [30–32]. By comparing all compositions, higher lattice strain values are obtained in the sample with 30% Si (Table 1). The difference in microstrain values were related to the Si segregation in grain boundaries, which made the growth of crystallites difficult. Moreover, lattice strains in crystallites are generated by structure defects in terms of vacancies, dislocations, stacking faults, and grain boundaries. Generally, dislocations density,  $\rho_s$ , can be represented in terms of the microstructural parameters, using the following equation cited in ref. [33]:

$$\rho_{bcc} = \frac{2\sqrt{3} \times (\varepsilon^2)^{1/2}}{D \times b} \quad (1)$$

where  $\varepsilon$  is the lattice strain,  $D$  is the crystallite size, and the Burgers vector of dislocations,  $b$ , equals  $a_{bcc} \frac{\sqrt{3}}{2}$  for the bcc structure.  $a_{bcc}$  is the lattice parameter fitted as a function of milling time for the bcc-structure. The calculated values of the dislocation densities,  $\rho_{bcc}$ , as a function of milling time are given in Table 1. As shown, with the increase in milling time, the  $\rho_{bcc}$  values increased for all sample compositions, and the highest value of  $17.5 \times 10^{15} \text{ m}^{-2}$  is identified for the case of the sample doped with 30%Si and milled for 100 h. Moreover, one can note an increase in the dislocation density when the Si content increases. This may be due to the hardening and brittleness of the material by the diffusion of Si in the grain boundaries. The latter are used as barriers to dislocation movement, in the sense that when they turn hard or contract, the number of dislocations near the grain boundaries will increase.

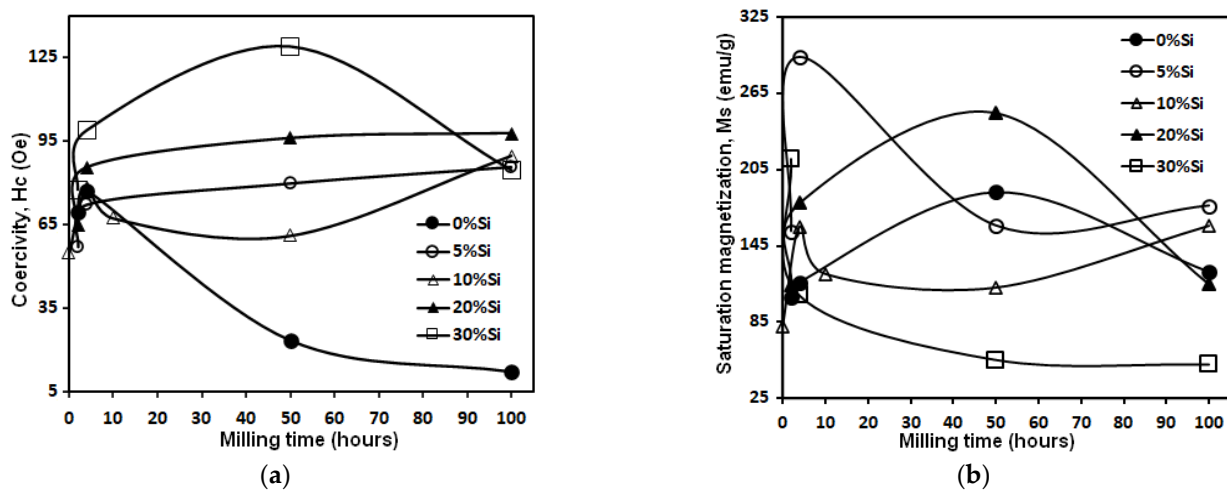
### 3.3. Magnetic Properties

Figure 4 gives a superposition of hysteresis loops of the powder mixtures without Si and containing 5, 10, 20, and 30 at% Si as a function of selected milling time. All the milled powders had similar hysteresis loops indicating that these samples have a ferromagnetic behavior.

Further, all hysteresis cycles exhibited a sigmoidal shape with weak loss. This latter is characteristic of behavior in nanostructured samples with small magnetic domains [33]. Moreover, these low hysteresis losses are properties demanded in soft magnetic compounds [34]. As the milling time increases, the cycles become flattened. This may be due to the very high value of the magnetostriction coefficient of these alloys which is of the order of  $\lambda_s = 2.5 \times 10^{-6}$  [35–38]. Moreover, the flattening of the hysteresis cycles of the powders when Si content increases can be explained by the decrease in coupling ferromagnetic.

The dependence of the coercivity ( $H_c$ ) and the saturation magnetization ( $M_s$ ) on the milling time are given in Figure 5. All mechanically alloyed powders have a soft magnetic behavior ( $H_c \leq 100 \text{ Oe}$ ) (Figure 5a). However, before 2 h of milling, an increase in  $H_c$  as a function of milling time and Si content additions of about 30 Oe is observed. This increase reflects the decrease in the coupling between ferromagnetic grains via the intergranular zone [39,40]. Based on the fact that the Fe, Co, and Ni alloys are ferromagnetic, the substitution of one of these elements by Si, which is not magnetic, leads to a decrease in ferromagnetic coupling [41]. However, it has been reported that dislocation density is the most important factor that affects coercivity [42]. Further, Yu et al. have observed

experimentally that the increase of  $H_c$  is directly linked to the presence of grain boundaries, precipitates, and disordered phases [43]. Another cause of increased  $H_c$  may be surface anisotropy [43–46]. This latter may have origins in the interactions of exchange between the spins of the core and surface atoms [44–47]. Indeed, by reducing the particle size down to the nanometric scale, the surface/volume ratio increases, and hence the influence of surface anisotropy increases [48,49]. Then again, for the FeCoNi alloy without Si, we can notice a decrease in  $H_c$  up to a value of 12.4 Oe at 100 h of milling. In addition, a slight decrease of 15 Oe for the sample with 10% Si between 4 and 50 h of milling is observed. The reduction of  $H_c$  can be attributed to the reduction of magnetic anisotropy. The start of milling is characterized by a decrease in the volume fraction of hcp-Co, hence a reduction in anisotropy magneto-crystalline.



**Figure 5.** The evolution of the coercivity ( $H_c$ ) (a) and the saturation magnetization ( $M_s$ ) (b) of the MA Fe<sub>60-x</sub>Co<sub>25</sub>Ni<sub>15</sub>Si<sub>x</sub> ( $x = 0, 5, 10, 20,$  and  $30$  at%Si) alloys on the milling time. (Units:  $1 \text{ Oe} = 10^{-4} \text{ T}$ ).

We recall that the hcp structures have a magneto-crystalline anisotropy higher than cubic structures [50]. In addition, the decrease in the coercive field,  $H_c$ , can also be related to the increase in the average particle size at the start of milling (by agglomeration). The particle size of powder results from the competition between the repeated phenomena of fracture and welding. With increasing particle size, the alloy becomes multi-domain, and the magnetization is done by displacement of walls. The magnetic softness is dependent on the reduction of residual tensions when the particle size increases [51,52].

The dependence of saturation magnetization ( $M_s$ ) on the milling time can provide additional information on the magnetic behavior during the MA process. As can be seen in Figure 5b,  $M_s$  strongly depends on the chemical composition of the alloys. After 4 h of milling, the  $M_s$  decrease (for samples with 5, 10, 30%Si content) can be explained by the segregation of Si in the FeCoNi lattice. After 100 h, the saturation magnetization takes very close values, while for the samples without Si and with 20%, one can observe an increase after 4 h followed by a decrease after 50 h of milling. The inhomogeneous evolution of  $M_s$  as a function of Si content can be linked to the magnetostriction effective anisotropy and stress introduced during the milling process. As a result, one can deduce that  $M_s$  is independent of the microstructure and strongly sensitive to the chemical composition; the opposite of coercivity  $H_c$ ,  $M_s$  is structure insensitive.

#### 4. Conclusions

Nanostructured Fe<sub>60-x</sub>Co<sub>25</sub>Ni<sub>15</sub>Si<sub>x</sub> ( $x = 0, 5, 10, 20,$  and  $30$  at%) alloys were prepared by a high-energy mechanical ball milling. Microstructural and magnetic properties as a function of milling time were investigated. The formation of the supersaturated Fe(Co,Ni,Si) solid solution was identified by the use of XRD diffractograms after 100 h of milling. The increase in the Si content favors the work hardening of powdered alloys resulting in



particle and crystallite size reduction and lattice strain rise. Increasing the milling time and adding Si into Fe, Co, and Ni mixture metals at the same time diminishes the Ms due to the microstructure refinement and Si diamagnetic effect. The final mechanically alloying products showed a soft magnetic behavior ( $H_c \leq 100$  Oe).

**Author Contributions:** Formal analysis: N.K., N.L.-I. and B.H.; supervision: J.-J.S. and M.K.; investigation: N.K. and W.B.M.; writing—original draft preparation: J.-J.S. and M.K. All authors have read and agreed to the published version of the manuscript.

**Funding:** This research received no external funding.

**Institutional Review Board Statement:** Not applicable.

**Informed Consent Statement:** Not applicable.

**Data Availability Statement:** Data can be requested to the authors.

**Conflicts of Interest:** The authors declare no conflict of interest.

## References

1. Laala-Bouali, H.; Bentayeb, F.Z.; Louidi, S.; Guo, X.; Tria, S.; Suñol, J.J.; Escoda, L. X-ray line profile analysis of the ball-milled Fe–30Co alloy. *Adv. Powder Technol.* **2013**, *24*, 168–174. [[CrossRef](#)]
2. Sathawong, R.; Koizumi, N.; Song, C.; Prasassarakich, P. Bimetallic Fe–Co catalysts for CO<sub>2</sub> hydrogenation to higher hydrocarbons. *J. CO<sub>2</sub> Util.* **2013**, *3*, 102–106. [[CrossRef](#)]
3. Raanaei, H.; Eskandari, H.; Mohammad-Hosseini, V. Structural and magnetic properties of nanocrystalline Fe–Co–Ni alloy processed by mechanical alloying. *J. Magn. Magn. Mater.* **2016**, *398*, 190–195. [[CrossRef](#)]
4. Li, X.; Takahashi, S. Synthesis and magnetic properties of Fe–Co–Ni nanoparticles by hydrogen plasma–metal reaction. *J. Magn. Magn. Mater.* **2000**, *214*, 195–203. [[CrossRef](#)]
5. Gupta, K.; Raina, K.K.; Sinha, S.K. Influence of process parameters and alloy composition on structural, magnetic and electrical characteristics of Ni–Fe permalloys. *J. Alloys Compd.* **2007**, *429*, 357–364. [[CrossRef](#)]
6. Handbook. A.S.M. *Metallography and Microstructures*; ASM International: Geauga County, OH, USA, 1995; p. 538.
7. Dietrich, D.W. *Magnetically Soft Materials, Properties and Selection: Non-ferrous Alloys Special-Purpose Materials*; ASM Handbook; ASM International: Geauga County, OH, USA, 1990; p. 761.
8. Jiles, D. *Introduction to Magnetism and Magnetic Materials*; Chapman and Hall: London, UK, 1991; pp. 280–297.
9. Lu, Z.; Li, H.; Lei, Z.; Chang, C.; Wang, X.; Lu, Z. The effects of metalloids elements on the nanocrystallization behavior and soft magnetic properties of FeCBSiPCu amorphous alloys. *Metals* **2018**, *8*, 283. [[CrossRef](#)]
10. Kim, Y.; Hwang, B. Effect of metalloids elements on the mechanical properties of Fe-based bulk amorphous alloys. *Korean J. Mater. Res.* **2016**, *26*, 671–675. [[CrossRef](#)]
11. Gorria, P.; Martínez-Blanco, D.; Pérez, M.J.; Blanco, J.A.; Hernando, A.; Laguna-Marco, M.A.; Haskel, D.; Souza-Neto, N.; Smith, R.I.; Marshall, W.G.; et al. Stress-induced large Curie temperature enhancement in Fe<sub>64</sub>Ni<sub>36</sub> Invar alloy. *Phys. Rev. B* **2009**, *80*, 064421. [[CrossRef](#)]
12. Zuo, T.T.; Li, R.B.; Ren, X.J.; Zhang, Y. Effects of Al and Si addition on the structure and properties of CoFeNi equal atomic ratio alloy. *J. Magn. Magn. Mater.* **2014**, *371*, 60–68. [[CrossRef](#)]
13. Zuo, T.; Gao, M.C.; Ouyang, L.; Yang, X.; Cheng, Y.; Feng, R.; Chen, S.; Liaw, P.K.; Hawk, J.A.; Zhang, Y. Tailoring magnetic behavior of CoFeMnNi<sub>X</sub> (X = Al, Cr, Ga, and Sn) high entropy alloys by metal doping. *Acta Mater.* **2017**, *130*, 10–18. [[CrossRef](#)]
14. Chen, C.; Wang, W.; Li, H.; Wei, P.; Zhang, W.; Fan, Y.; Chen, J.; Yuan, S.; Wei, R.; Zhang, T.; et al. Effects of Al and Mn on microstructure, magnetic and mechanical properties of Fe<sub>40</sub>Co<sub>40</sub>Ni<sub>10</sub>M<sub>10</sub> (M = Al, Mn) medium entropy alloys. *J. Alloys Compd.* **2022**, *890*, 161779. [[CrossRef](#)]
15. Chang, T.; Zou, C.M.; Zhu, D.D.; Wang, X.H.; Wei, Z.J.; Wang, H.W.; Fang, N.; Chen, J.H. Microstructure and magnetic behaviors of FeCoNi (Al) alloys with incoherent nanoprecipitates prepared by high-pressure solidification. *J. Alloys Compd.* **2022**, *894*, 162501. [[CrossRef](#)]
16. Feng, W.; Qi, Y.; Wang, S. Effects of Mn and Al addition on structural and magnetic properties of FeCoNi-based high entropy alloys. *Mater. Res. Express.* **2018**, *5*, 106511. [[CrossRef](#)]
17. Li, Z.; Qi, J.; Li, Z.; Li, H.; Xu, H.; Bai, G.; Liu, X.; Zhang, X. Effect of grain and phase boundaries on soft magnetic properties of FeCoNiAlSi high-entropy alloys. *Mater. Lett.* **2021**, *297*, 129965. [[CrossRef](#)]
18. Kulkarni, R.; Murty, B.S.; Srinivas, V. Study of microstructure and magnetic properties of AlNiCo(CuFe) high entropy alloy. *J. Alloys Compd.* **2018**, *746*, 194–199. [[CrossRef](#)]
19. Alijani, V.; Winterlik, J.; Fecher, G.H.; Naghavi, S.S.; Felser, C. Quaternary half-metallic Heusler ferromagnets for spintronics applications. *Phys. Rev. B* **2011**, *83*, 184428. [[CrossRef](#)]
20. Prasad, N.K.; Kumar, V. Structure–magnetic properties correlation in mechanically alloyed nanocrystalline Fe–Co–Ni–(Mg–Si)<sub>x</sub> alloy powders. *J. Mater. Sci. Mater. Electron.* **2016**, *27*, 10136–10146. [[CrossRef](#)]

21. Yuping, D.; Yahong, Z.; Tongmin, W.; Shuchao, G.; Xingjun, L. Evolution study of microstructure and electromagnetic behaviors of Fe–Co–Ni alloy with mechanical alloying. *Mater. Sci. Eng. B* **2014**, *185*, 86–93. [[CrossRef](#)]
22. Sahu, P.; Solanki, S.; Dewangan, S.; Kumar, V. Microstructure and magnetic behavior of FeCoNi (Mn–Si)<sub>x</sub> (x = 0.5, 0.75, 1.0) high-entropy alloys. *J. Mater. Res.* **2019**, *34*, 829–840. [[CrossRef](#)]
23. Khitouni, N.; Daly, R.; Escoda, L.; Llorca-Isern, N.; Suñol, J.J.; Dammak, M.; Khitouni, M. The Effect of B and Si Additions on the Structural and Magnetic Behavior of Fe-Co-Ni Alloy Prepared by High-energy Mechanical Milling. *J. Supercond. Nov. Magn.* **2020**, *33*, 2727–2735. [[CrossRef](#)]
24. Carrillo, A.; Escoda, L.; Saurina, J.; Suñol, J.J. Structural and Magnetic behavior of Fe(Nb,Zr) rich alloys produced by mechanical alloying. *AIP Adv.* **2018**, *8*, 047704. [[CrossRef](#)]
25. Lutterotti, L. *MAUD CPD Newsletter*; IUCr: Chester, UK, 2000; p. 24.
26. Suryanarayana, C.; Ivanov, E.; Boldyrev, V.V. The science and technology of mechanical alloying. *Mater. Sci. Eng. A* **2001**, *304*, 151–158. [[CrossRef](#)]
27. Koch, C.C. Top-Down Synthesis of Nanostructured Materials: Mechanical and Thermal Processing Methods. *Rev. Adv. Mater. Sci.* **2003**, *5*, 91–99.
28. Khajepour, M.; Sharafi, S. Characterization of nanostructured Fe–Co–Si powder alloy. *Powder Technol.* **2012**, *232*, 124–133. [[CrossRef](#)]
29. Chitsazan, B.; Shokrollahi, H.; Behvandi, A.; Mirzaee, O. Characterization and magnetic coercivity of nanostructured (Fe<sub>50</sub>Co<sub>50</sub>)<sub>100-x</sub>V<sub>x=0,2,4</sub> powders containing a small amount of Co<sub>3</sub>V intermetallic obtained by mechanical alloying. *Powder Technol.* **2011**, *214*, 105–110. [[CrossRef](#)]
30. Mhadhbi, M.; Khitouni, M.; Escoda, L.; Suñol, J.J. X-ray studies of structure defects in nanostructured FeAl alloy. *Mater. Lett.* **2010**, *64*, 1802–1805. [[CrossRef](#)]
31. Mohamed, F.A. A dislocation model for the minimum grain size obtainable by milling. *Acta Mater.* **2003**, *51*, 4107–4119. [[CrossRef](#)]
32. Kalita, M.P.; Perumal, A.; Srinivasan, A. Structure and magnetic properties of nanocrystalline Fe<sub>75</sub>Si<sub>25</sub> powders prepared by mechanical alloying. *J. Magn. Magn. Mater.* **2008**, *320*, 2780–2783. [[CrossRef](#)]
33. Daly, R.; Sunol, J.J.; Khitouni, M. Structural thermal properties of the Fe-based alloys prepared by mechanical milling Korean. *J. Chem. Eng.* **2022**, *39*, 1614–1623.
34. Souilah, S.; Alleg, S.; Djebbari, C.; Ben Salema, R.; Sunol, J.J. Magnetic and microstructural properties of the mechanically alloyed Fe<sub>57</sub>Co<sub>21</sub>Nb<sub>7</sub>B<sub>15</sub> powder mixture. *Mater. Chem. Phys.* **2012**, *132*, 766–772. [[CrossRef](#)]
35. Yousefi, M.; Sharafi, S.; Mehrolohosseiny, A. Correlation between structural parameters and magnetic properties of ball milled nano-crystalline Fe–Co–Si powders. *Adv. Powder Technol.* **2014**, *25*, 752–760. [[CrossRef](#)]
36. Gercsi, Z.; Mazaleyrat, F.; Kane, S.N.; Varga, L.K. Magnetic and structural study of (Fe<sub>1-x</sub>Co<sub>x</sub>)<sub>62</sub>Nb<sub>8</sub>B<sub>30</sub> bulk amorphous alloys. *Mater. Sci. Eng. A* **2004**, *375*, 1048–1052. [[CrossRef](#)]
37. McHenry, M.E.; Willard, M.A.; Laughlin, D.E. Amorphous and nanocrystalline materials for applications as soft magnets. *Prog. Mater. Sci.* **1999**, *44*, 291–433. [[CrossRef](#)]
38. Alves, F.; Simon, F.; Kane, S.N.; Mazaleyrat, F.; Waeckerle, T.; Save, T.; Gupta, A. Influence of rapid stress annealing on magnetic and structural properties of nanocrystalline Fe<sub>74.5</sub>Cu<sub>1</sub>Nb<sub>3</sub>Si<sub>15.5</sub>B<sub>6</sub> alloy. *J. Magn. Magn. Mater.* **2005**, *294*, e141–e144. [[CrossRef](#)]
39. Daly, R.; Khitouni, N.; Escoda, M.L.; Isern, N.L.; Sunol, J.J.; Greneche, J.M.; Khitouni, M. Microstructure, Magnetic and Mössbauer Studies of Mechanically Alloyed FeCoNi Nanocrystalline Powders. *Arab. J. Sci. Eng.* **2021**, *46*, 5633–5643. [[CrossRef](#)]
40. Schrefl, T.; Fidler, J.; Kronmüller, H. Remanence and coercivity in isotropic nanocrystalline permanent magnets. *Phys. Rev. B* **1994**, *49*, 6100. [[CrossRef](#)]
41. Jurczyk, M. Nanocomposite Nd–Fe–B type magnets. *J. Alloys Compd.* **2000**, *299*, 283–286. [[CrossRef](#)]
42. Kaczmarek, K.; Pierre, J.; Tobola, J.; Skolozdra, R.V. Anderson localization of 3 d Mn states in semi-Heusler phases. *Phys. Rev. B* **1999**, *60*, 373. [[CrossRef](#)]
43. Shen, T.D.; Schwarz, R.B.; Thompson, J.D. Soft magnetism in mechanically alloyed nanocrystalline materials. *Phys. Rev. B* **2005**, *72*, 014431. [[CrossRef](#)]
44. Yu, R.H.; Basu, S.; Ren, L.; Zhang, Y.; Parvizi-Majidi, A.; Unruh, K.M.; Xiao, J.Q. High temperature soft magnetic materials: FeCo alloys and composites. *IEEE Trans. Magn.* **2000**, *36*, 3388–3393. [[CrossRef](#)]
45. Luis, F.; Torres, J.M.; García, L.M.; Bartolomé, J.; Stankiewicz, J.; Petroff, F.; Fetta, F.; Maurice, J.L.; Vaures, A. Enhancement of the magnetic anisotropy of nanometer-sized Co clusters: Influence of the surface and of interparticle interactions. *Phys. Rev. B* **2002**, *65*, 094409. [[CrossRef](#)]
46. Chen, J.P.; Sorensen, C.M.; Klabunde, K.J.; Hadjipanayis, G.C. Enhanced magnetization of nanoscale colloidal cobalt particles. *Phys. Rev. B* **1995**, *51*, 11527. [[CrossRef](#)]
47. Jamet, M.; Wernsdorfer, W.; Thirion, C.; Mailly, D.; Dupuis, V.; Mélinon, P.; Pérez, A. Magnetic anisotropy of a single cobalt nanocluster. *Phys. Rev. Lett.* **2001**, *86*, 4676. [[CrossRef](#)]
48. Dimian, M.; Kachkachi, H. Effect of surface anisotropy on the hysteretic properties of a magnetic particle. *J. Appl. Phys.* **2002**, *91*, 7625–7627. [[CrossRef](#)]
49. Crisan, O.; Angelakeris, M.; Flevaris, N.K.; Filoti, G. Magnetism and anisotropy in core-shell nanoparticles. *J. Optoelectron. Adv. Mater.* **2003**, *5*, 959–962.

50. Muroi, M.; McCormick, P.G.; Street, R. Surface spin disorder and exchange bias in  $\text{La}_{0.7}\text{Ca}_{0.3}\text{MnO}_3$  nanoparticles synthesised by mechanochemical processing. *Rev. Adv. Mater. Sci.* **2003**, *5*, 76–81.
51. Weller, D.; Harp, G.R.; Farrow, R.F.; Cebollada, A.; Sticht, J. Orientation dependence of the polar Kerr effect in fcc and hcp Co. *Phys. Rev. Lett.* **1994**, *72*, 2097. [[CrossRef](#)]
52. Blázquez, J.S.; Franco, V.; Conde, C.F.; Conde, A. Nanocrystalline Fe–Nb–(B, Ge) alloys from ball milling: Microstructure, thermal stability and magnetic properties. *Intermetallics* **2007**, *15*, 1351–1360. [[CrossRef](#)]